



Photonic millimeter-wave generation beyond the cavity thermal limit

WILLIAM GROMAN,^{1,2,3,*} IGOR KUDELIN,^{1,2,3} ALEXANDER LIND,^{1,3} DAHYEON LEE,^{2,3} TAKUMA NAKAMURA,³ YIFAN LIU,^{2,3} MEGAN L. KELLEHER,^{2,3} CHARLES A. MCLEMORE,^{2,3} JOEL GUO,⁴ LUE WU,⁵ WARREN JIN,⁴ KERRY J. VAHALA,⁵ JOHN E. BOWERS,⁴ FRANKLYN QUINLAN,^{1,3} AND SCOTT A. DIDDAMS^{1,2,3}

¹Electrical Computer & Energy Engineering, University of Colorado, Boulder, Boulder, Colorado 80309, USA

²Department of Physics, University of Colorado, Boulder, 440 UCB, Boulder, Colorado 80309, USA

³National Institute of Standards and Technology, 325 Broadway, Boulder, Colorado 80305, USA

⁴Department of Electrical and Computer Engineering, University of California, Santa Barbara, Santa Barbara, California 93106, USA

⁵T. J. Watson Laboratory of Applied Physics, California Institute of Technology, Pasadena, California 91125, USA

*william.groman@colorado.edu

Received 15 July 2024; revised 3 October 2024; accepted 4 October 2024; published 14 November 2024

Next-generation communications, radar, and navigation systems will extend and exploit the higher bandwidth of the millimeter-wave domain for increased communication data rates as well as radar with higher sensitivity and increased spatial resolution. However, realizing these advantages will require the generation of millimeter-wave signals with low phase noise in simple and compact form-factors. Photonic integration addresses this challenge and provides a path toward simplified and portable, low-noise mm-wave generation. We leverage these advances by heterodyning two silicon photonic chip lasers, phase-locked to different axial modes of a miniature Fabry–Perot (F-P) cavity to demonstrate a simple framework for generating low-noise millimeter-waves. By reducing technical noise, we achieve common-mode rejection of the thermally driven Brownian noise such that the millimeter-wave phase noise surpasses that of the thermal limit of a single laser locked to the F-P cavity. This leads to a 118.1 GHz millimeter-wave signal with phase noise of -118 dBc/Hz at 10 kHz offset, decreasing to -120 dBc/Hz at 30 kHz offset. We achieve this with technologies that can be integrated into a platform less than ≈ 10 mL. Our work overcomes fundamental thermal-mechanical noise limits intrinsic to integrated photonics, while illustrating advantages of the same for providing low-size, -weight, and -power (SWaP) mm-waves that will be enabling for multiple applications in communications and sensing. © 2024 Optica Publishing Group under the terms of the Optica Open Access Publishing Agreement

https://doi.org/10.1364/OPTICA.536549

1. INTRODUCTION

Inherent in the higher frequency of millimeter-wave carriers (mm-wave, $\approx 30 \rightarrow 300$ GHz) is the capability of higher modulation bandwidth and faster data transfer rates [1,2], finer radar and sensing spatial resolution [3,4], antenna miniaturization [3], and the potential for effective atmospheric transmission. [5]. The impact of mm-waves is already evident in cutting-edge telecommunications, with 5G utilizing carriers in both the microwave and low mm-wave range ($\lesssim 50$ GHz), and 6G technology pushing carrier frequencies beyond 90 GHz [6]. Furthermore, mm-wave technologies have already shown promise for safe and non-invasive biomedical and security sensing applications [7,8], and are widely used as radio astronomy references [9].

In the microwave range, rack-mount-volume synthesizers dominate the application space. These provide wide tunability, but with close-to-carrier phase noise that, in the best case, is given by a frequency-multiplied quartz reference or other dielectric oscillator. Such signal sources are commonly extended to the mm-wave via

carrier multiplication by N , but that comes with additional degradation in phase noise power spectral density by at least $20 \log(N)$ [10]. As a result, commercial mm-wave synthesizers at 100 GHz are typically limited in phase noise performance in the range of -100 dBc/Hz at 10 kHz offset and often fall short in meeting the demands as local oscillators (LOs) in the aforementioned radar and telecommunication applications. On the other hand, laboratory research synthesizers provide remarkably low noise at the cost of increasing complexity and larger volume [11].

Within this context, the field of mm-wave photonic synthesis with narrow-linewidth lasers provides a compelling alternative to electronic approaches. Most simply, the interference of two continuous wave (CW) lasers can be photomixed (photodetected) to produce a mm-wave signal at the difference frequency of the lasers. This concept was first demonstrated just a few years after the invention of the laser, but progress has accelerated over the past two decades with multiple techniques involving lasers, electro-optics, and frequency combs to generate and control the relative frequency difference between the CW lasers [12–20].

Even greater opportunities for photonic mm-waves are offered by the confluence of recent advances in chip-integrated low-noise lasers and frequency combs and the means to frequency-stabilize these light sources with compact, high-finesse, and integrable high-Q optical cavities. Importantly, lasers can now be heterogeneously integrated on a CMOS-compatible platform together with extremely low-loss Si_4N_3 ring resonators for self-injection locking (SIL) operation [21,22]. This leads to laser frequency noise that is typically associated with narrow-linewidth fiber lasers, but with a smaller footprint [23]. In addition, miniaturization and integration of centimeter-sized optical cavities with finesse approaching 10^6 [24,25] transforms the realization of hertz-linewidth lasers from large laboratory setups to the chip-scale, and in some cases even forgoing the need for vacuum enclosures [25]. Recent combinations of such integrated photonic hardware have further utilized the powerful approach of optical frequency division (OFD) for low-noise microwave and mm-wave generation [26,27].

In this work, we show that the benefits of OFD are not required to further advance the phase noise of mm-wave generation at 100 GHz and above. Instead we exploit the high degree of thermal noise correlation and common-mode noise rejection between the axial modes of a Fabry–Perot (F-P) to strongly reject this noise in mm-wave generation. A cavity Q-factor approaching 10^{10} and linewidth near 20 kHz allow us to tightly lock the frequencies of two lasers to cavity modes with residual noise that is well below the room-temperature cavity thermal noise. Thus, the correlated thermal noise of the cavity close-to-carrier that is imprinted on each laser is subtracted in the mm-wave heterodyne beat.

We implement this concept with two SIL lasers that are frequency-locked to modes of a miniature high-Q Fabry–Perot cavity with free spectral range, $\text{FSR} = 23.6$ GHz. For modes separated by $5 \times \text{FSR} = 118$ GHz, the phase noise of the heterodyne beat is -118 dBc/Hz at 10 kHz offset, decreasing to -120 dBc/Hz at 30 kHz. Importantly, our approach uses the same components that have been shown to be compatible with chip-scale integration, while offering phase noise levels that match those achieved with more complicated integrated OFD approaches. And at 10 kHz offset our results are close to the noise levels achieved in the very best photonic mm-wave laboratory experiments.

Our straightforward approach to mm-wave generation effectively removes the fundamental limitations imposed by cavity thermal noise. As such, we anticipate that further improvements in phase noise performance will be allowed to proceed at the more rapid pace of technical innovations in low-noise chip-integrated lasers and frequency control techniques.

2. CONCEPT AND EXPERIMENT

Figure 1(a) shows a simplified schematic of the experiment. Starting from the left, two distributed-feedback (DFB) lasers (ν_1 and ν_2) are individually coupled and self-injection locked to separate high-Q ($Q \gtrsim 10^8$) Si_3N_4 microresonators, with free spectral ranges (FSRs) of about 135 MHz. The self-injection locking is controlled by fine-tuning the facet distance, and thereby the phase, of the DFBs relative to their respective microresonator chips, and results in a phase noise suppression of the free-running DFB signal by up to 50 dB [28]. The SIL laser output is then fiber-coupled out of the chip for use.

This initial self-injection locking suppresses the close-to-carrier noise and allows us to use the Pound–Drever–Hall (PDH)

technique [29] to subsequently lock each laser's frequency to an ultra-stable, temperature- and vacuum-controlled, miniature F-P cavity. In this case, the laser frequency inherits the stability of the cavity, but with frequency noise fundamentally limited by thermally driven stochastic fluctuations in the cavity length [30]. Here, the cavity we used is exhibited and referred to in [31] as the “all-ULE cavity”. We lock both lasers to separate F-P cavity modes such that the mm-wave carrier frequency is $f_\mu = n \times \text{FSR} = \nu_1 - \nu_2$, as portrayed in Fig. 1(c). Importantly, subtraction of these two PDH-locked signals, as occurs in photodetection, results in noise cancellation of the common noise, including thermal noise inherited by both lasers from the cavity. This yields an output signal with phase noise below that of the cavity thermal limit.

Figure 1(b) illustrates the primary noise contributions to f_μ and their subtraction in the time domain. The two PDH-locked lasers have frequency fluctuations dominated by two terms: the intrinsic cavity thermal noise σ_{th} and the smaller residual noise of the PDH lock σ_{PDH} that is related to technical servo limitations. Because of significant overlap of the spatial modes of ν_1 and ν_2 in the F-P cavity, there is strong amplitude and phase correlation between $\sigma_{\text{th}}^{(1)}$ and $\sigma_{\text{th}}^{(2)}$. In the heterodyne, these noise terms largely subtract, as shown in the bottom of Fig. 1(b). However, the PDH locking noise $\sigma_{\text{PDH}}^{(1)}$ and $\sigma_{\text{PDH}}^{(2)}$ arises from uncorrelated noise from the separate laser locks and instead adds in quadrature in the heterodyne signal, such that $\sigma_\mu^2 = (\sigma_{\text{PDH}}^{(1)})^2 + (\sigma_{\text{PDH}}^{(2)})^2$.

The extent of the rejection of the correlated (common-mode) noise can be estimated by considering the fractional frequency stability that one laser inherits from the cavity, and extending the argument to two lasers separated by n modes. The magnitude of the thermally driven fluctuations of a frequency mode ν of the cavity is directly linked to the fluctuations of the cavity FSR, such that $\sigma_{\text{FSR}} = (\text{FSR}/\nu)\sigma_\nu$. Here we see that the frequency fluctuations σ_ν of mode ν are ideally reduced by the ratio of $\text{FSR}/\nu \approx 10^{-4}$. Similarly, $\sigma_{n \times \text{FSR}} = (n \times \text{FSR}/\nu)\sigma_\nu$, where $n \times \text{FSR}$ is the separation of any two modes of the cavity [25]. Considering two lasers locked to modes separated by $5 \times \text{FSR} = 118$ GHz, the expected common rejection of frequency fluctuations is 6×10^{-4} , which is equivalent to a reduction of $20 \cdot \log(118 \text{ GHz}/193 \text{ THz GHz}) \approx -64$ dB in phase noise power spectral density [25]. This estimate assumes perfect correlation of thermal noise in the two cavity modes, and therefore neglects the slight variations in cavity mode volume with wavelength. But for two nearby axial modes, this approximation sufficiently justifies how the phase noise of the mm-wave beat can surpass the cavity thermal limit. It is then limited by the PDH locking noise of the lasers, which can be addressed through technical advances.

In the experiment, the two PDH-locked lasers are mixed on a commercial W-band photodetector and the resulting output is a millimeter-wave (“output” in Fig. 1), having power of ≈ 1 mW. Here, we demonstrate millimeter-wave signals at $4 \times \text{FSR}$ and $5 \times \text{FSR}$, with 94.5 GHz and 118.1 GHz carriers, respectively. The phase noise of the millimeter-wave signals was measured using cross correlation techniques to remove the uncorrelated noise of reference local oscillators, as well as the mixer and amplifier noise [32]. In brief, the photodetected signal was split with a -3 dB waveguide coupler and each copy was mixed down to the RF using harmonic mixers driven by independent commercial synthesizers. The two resulting baseband signals near 5 MHz were then cross-correlated on a phase noise analyzer.

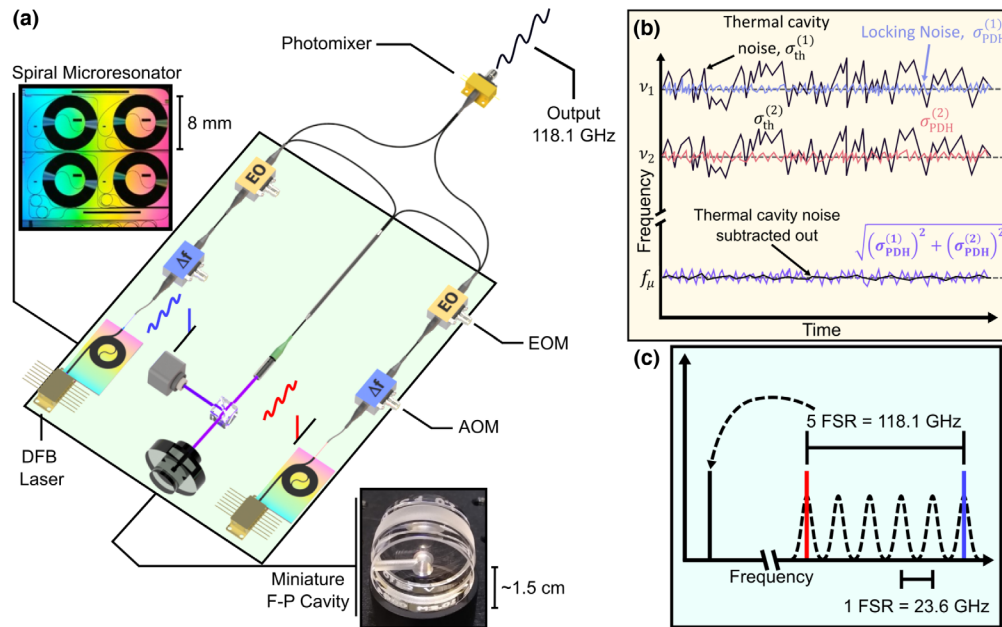


Fig. 1. (a) Simplified schematic of the experiment, with pictures of the key components zoomed in. (b) Illustration of the mechanism of common-mode rejection. Two signals (ν_1 and ν_2) are indicated by their nominal frequencies (gray dashed lines) with their noise contributions (the thermal cavity noise of each laser, $\sigma_{th}^{(1)}$ and $\sigma_{th}^{(2)}$, as well as PDH locking noise, $\sigma_{PDH}^{(1)}$ and $\sigma_{PDH}^{(2)}$, respectively) shown as continuous lines. The signal that results from their heterodyning, ν_{RF} , is shown with the thermal cavity noise largely subtracted out. (c) Illustration of the two laser signals (red and blue) locked to two cavity modes (dashed Gaussians), and heterodyned at 5 cavity FSRs apart, to generate a 118.1 GHz RF tone.

3. RESULTS

The result of the cross-correlation phase noise measurements of the millimeter-wave signals is plotted in Fig. 2 (Cross-correlation measurement details, Supplement 1, Note 2). We see three overlaid traces of approximately the same phase noise level as the 1 FSR (23.6 GHz, blue), 4 FSR (94.5 GHz, yellow), and 5 FSR (118.1 GHz, red) signals. This indicates that the phase noise of any millimeter-wave signal of integer-multiple FSR frequency can be generated and will inherit the phase noise of the PDH-locked SIL lasers. The only limiting factor then is the power on the high-speed photodetector, and hence the signal-to-noise ratio, of the heterodyned signals as the frequency difference between the two lasers is increased. The discrepancies in the phase noise of the 118.1 GHz signal versus the 23.6 GHz signal (near 10 kHz offset) arise from the requirement of longer averaging times due to the noise constraints of the cross-correlation reference signals.

Lastly and for comparison, on the same plot we have plotted (in green) the cumulative noise contributions from the PDH servos that we measure independently and add in quadrature. The various noise contributions before summing can be seen in Supplement 1, Note 3. These sources include the in-loop phase noise of each SIL laser during PDH-lock operation, and the SNR floor of each PDH servo loop. First, we measure the in-loop phase noise of the error signal from the PDH reflection photodetector while the laser is PDH-locked. Then we scale this noise appropriately with the linewidth of the cavity and the slope of the PDH-lock error signal [33] Similarly, we measure the electronic servo noise floor by tuning the laser off resonance and measuring the phase noise of the error signal output. This gives us the expected electronic noise floor of the photodetector and servo in-loop while light is incident on the detector but not on resonance. This is also scaled according to the cavity linewidth and error signal slope. The result is four measurements (two from each laser) that are summed in quadrature.

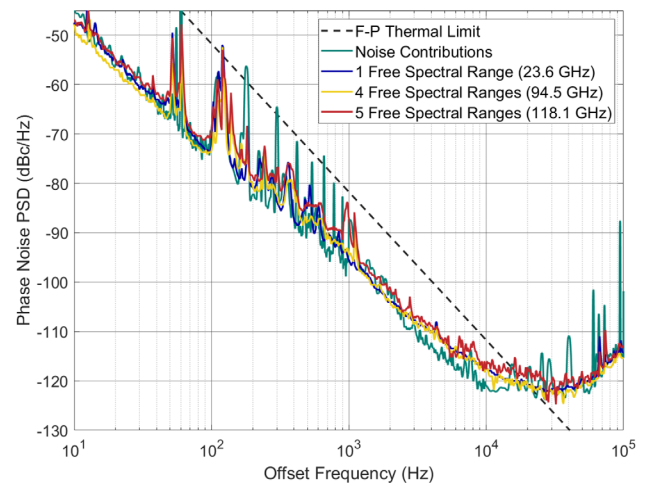


Fig. 2. Phase noise plot of the 1 FSR apart (23.6 GHz, Blue), 4 FSR apart (94.5 GHz, Yellow), and 5 FSR apart (118.1 GHz, Red) signals generated from heterodyning two self-injection-locked distributed feedback lasers after PDH locking to two modes of the miniature F-P. In green, the phase noise of the cumulative noise contributions is plotted, extrapolated from the PDH-locked laser in-loop noise.

We find that the integrated phase noise of the green curve agrees within a factor of 1.5 of the integrated phase noise of the 1 FSR, 4 FSR, and 5 FSR phase noise. Consequently, lower-phase-noise lasers or higher PDH-lock gain would offer even greater noise reduction.

In Fig. 3, we have plotted the free-running (without PDH locking) SIL laser phase noise (blue) and the 118.1 GHz signal phase noise (red), side-by-side, showing that ≈ 37 dB of noise reduction at 10 kHz offset is achieved by PDH locking, with AOM and EOM feedback, to the F-P cavity. (For Allan deviation of the

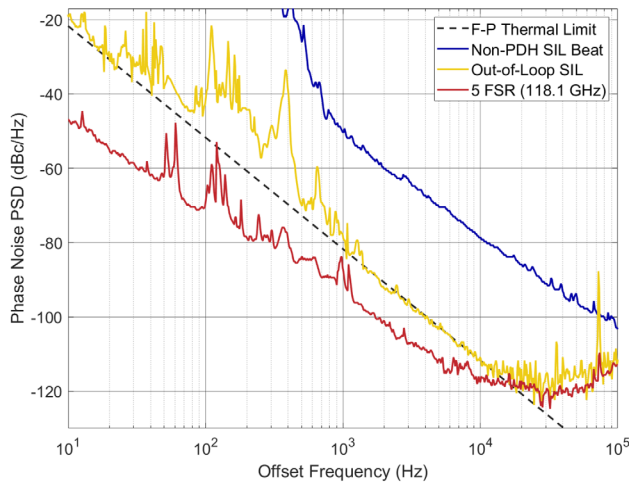


Fig. 3. Phase noise plot of the PDH-locked (yellow) versus unlocked (blue) SIL lasers, both measured out of loop. In red, the heterodyned millimeter wave at 5 FSR (118.1 GHz) separation is shown. In black-dashed line, the F-P cavity thermal limit referenced from [31] is plotted.

out-of-loop SIL and mmWave, see Supplement 1, Note 1.) Here we measured the free-running SIL noise by heterodyning the two SIL lasers on an MUTC with ≈ 10 GHz frequency difference. The 10 GHz signal is mixed down to DC and measured against a maser reference on a phase noise analyzer. We make the assumption that both free-running SIL lasers have similar but uncorrelated noise profiles, such that this phase noise is simply twice (+3 dB) that of a single SIL laser.

We also plotted the calculated thermal noise floor of the F-P cavity in dashed-black [31]. Comparing the thermal limit to the 118.1 GHz millimeter-wave signal reveals that for offset frequencies below 10 kHz, the phase noise of the millimeter-wave signal surpasses the thermal-limited optical phase noise over a wide range of Fourier frequencies. To further quantify the amount of common-mode rejection exhibited, we independently measured the absolute (out-of-loop) phase noise of an individual PDH-locked SIL laser (yellow in Fig. 3) by heterodyning with a lower-phase-noise cavity-referenced laser. As expected, we see that SIL laser noise follows the thermal limit of the F-P cavity up to about 10 kHz. At higher frequencies, the laser noise is limited by PDH servo gain and bandwidth.

The difference between the out-of-loop optical phase noise and the mm-wave phase noise is the amount of noise common to both lasers and hence subtracted (rejected) in the heterodyne signal, which is both the thermal noise of the cavity and vibration-induced noise of the cavity. Thus the mm-wave signal here gains 22 dB of noise rejection at 10 Hz offset, due to both optical references being PDH-locked to the same cavity.

To put our result into context, we have included a survey of the reported phase noise of state-of-the-art photonic millimeter-wave synthesis. As seen in Fig. 4, our SIL and PDH framework allows for exceptionally low-noise millimeter-wave synthesis, largely falling well below commercial products and existing photonic-based sources up until the servo bump at around 300 kHz. This does not tell the full story, however, as other millimeter-wave generators rely on significantly more complex systems or non-integratable components, to achieve lower and similar phase noise.

For example, the lowest phase noise achieved and plotted in red squares, incorporates full optical frequency division using an octave spanning, titanium-doped sapphire, bulk-optic frequency

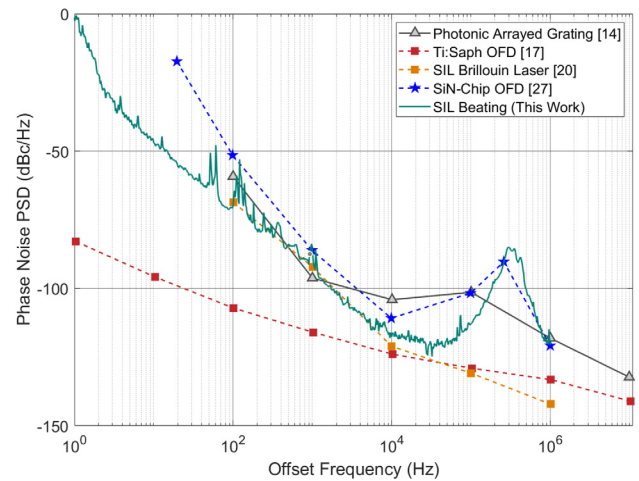


Fig. 4. Phase noise plot of the photonic millimeter-wave landscape scaled to 118.1 GHz [14,17,20,27].

comb and a filtering etalon [17]. The power required to run such a system is thus significantly higher than the one in this work. The lowest photonic-chip-based mm-wave noise (blue stars) falls in line with the results we present, yet they require a microcomb to achieve OFD [27]. In addition to the microcomb, this requires a more complex locking scheme. A more recent work from the same group has offered further simplification by using OFD with an injection-locked comb [34]. With the exception of additional spurious noise, these latest results are still comparable to what we present here, with noticeably reduced phase noise and a servo bump extended out to 500 kHz. Significantly, we have shown that such phase noise levels can be achieved without OFD using simple SIL lasers that require low input currents (200 mA to drive the lasers) and have a clear path toward chip integration.

The phase noise survey also includes other mm-wave synthesizers that employ self-injection locking with diode lasers (gray triangles) [14] and Brillouin lasers (orange squares) [20]. In the dual-wavelength Brillouin architecture, a 75-m-long fiber spool is used as a common cavity for self-injection locking two lasers.

In our data of Fig. 4, we see that there is excess noise arising from the servo bumps spanning 100 kHz to 1 MHz. This noise is attributed to the phase roll-off and limited gain of the laser control servo electronics. To mitigate this noise, one could implement servo control electronics with higher phase roll-off or an electro-optic modulator as an additional actuator [35].

There are additional spurious tones at 100–400 Hz in the out-of-loop PDH-locked laser phase noise of Fig. 3. These are also evident, at reduced amplitude, in the phase noise of the 118.1 GHz signal. Presumably, these arise from mechanical noise of the optomechanical stages that the lasers and chips reside on, as well as excess fiber noise. Additionally, some of these peaks likely originate from AM-PM conversion due to the relative intensity noise of the lasers.

4. CONCLUSION AND OUTLOOK

In conclusion, we have shown a simplified, compact way to generate low-phase-noise millimeter-wave carriers, by transferring the noise of stable optical references to any integer multiple of the F-P cavity FSR. Importantly, through common-mode rejection, we surpass the thermal limit of the reference cavity. In doing so, we have shown millimeter-wave phase noise of -118 dBc/Hz

at 10 kHz offset, regardless of carrier frequency. This performance is better than any chip-scale photonic mm-wave generation to date, and is within 5 dB the highest-performing full-OFD millimeter-wave source.

In addition to the phase noise performance, the low complexity and compact form factor of this experiment both lend themselves towards full integration. For example, with advances of micro-F-P cavities [24,25,36], integrated SIL lasers, and on-chip MUTC photodetectors [22,37], the approach we present can be integrated onto a single chip. And in comparison to more complex OFD schemes [26,27], we show an attractive option to reduce the number of integrated components and realize on-chip, low-noise mm-wave generation with robust and turn-key operation.

Funding. National Institute of Standards and Technology (80NM0018D0004); Defense Advanced Research Projects Agency GRYPHON program (HR0011-22-2-0009).

Acknowledgment. W.G., I.K., K.J.V, J.E.B., F.Q., and S.A.D. conceived the experiment and supervised the project. W.G., I.K., and S.A.D. wrote the paper with input from all authors. W.G., I.K., and A.L. built the experiment and performed the mm-wave experiment. D.L., T.N., and Y.L. provided mm-wave reference sources and input regarding the cavity and cross-correlation measurements. M.L.K and C.A.M. built the cavity and provided information regarding the cavity. J.G., L.W., W.J., K.J.V, and J.E.B provided the lasers and spiral microresonators, as well as input regarding the operation of the lasers.

Disclosures. The authors declare no conflicts of interest. Commercial equipment and trade names are identified for scientific clarity only and do not represent an endorsement by NIST.

Data availability. Data underlying the results presented in this paper are not publicly available at this time but may be obtained from the authors upon reasonable request.

Supplemental document. See Supplement 1 for supporting content.

REFERENCES

- J. Ma, R. Shrestha, L. Moeller, *et al.*, "Invited article: channel performance for indoor and outdoor terahertz wireless links," *APL Photonics* **3**, 051601 (2018).
- I. F. Akyildiz, J. M. Jornet, and C. Han, "Terahertz band: next frontier for wireless communications," *Phys. Commun.* **12**, 16–32 (2014).
- A. Soumya, C. K. Mohan, and L. R. Cenkeramaddi, "Recent advances in mmwave-radar-based sensing, its applications, and machine learning techniques: a review," *Sensors* **23**, 8901 (2023).
- T. S. Rappaport, Y. Xing, O. Kanhere, *et al.*, "Wireless communications and applications above 100 GHz: opportunities and challenges for 6G and beyond," *IEEE Access* **7**, 78729–78757 (2019).
- T. S. Rappaport, S. Sun, R. Mayzus, *et al.*, "Millimeter wave mobile communications for 5G cellular: it will work!" *IEEE Access* **1**, 335–349 (2013).
- W. Hong, Z. H. Jiang, C. Yu, *et al.*, "The role of millimeter-wave technologies in 5G/6G wireless communications," *IEEE J. Microwaves* **1**, 101–122 (2021).
- H. Wang, L. Lu, P. Liu, *et al.*, "Millimeter waves in medical applications: status and prospects," *Intell. Med.* **4**, 16–21 (2023).
- A. Luukanen, R. Appleby, M. Kemp, *et al.*, *Millimeter-Wave and Terahertz Imaging in Security Applications* (Springer Berlin Heidelberg, 2013), pp. 491–520.
- S. Doeleman, "High frequency very long baseline interferometry: frequency standards and imaging an event horizon," in *Frequency Standards and Metrology* (World Scientific, 2009), pp. 175–183.
- R. Bara-Maillet, S. R. Parker, N. R. Nand, *et al.*, "Microwave-to-millimeter-wave synthesis chain phase noise performance," *IEEE Trans. Ultrason. Ferroelectr. Freq. Control* **62**, 1895–1900 (2015).
- R. Bara, J.-M. L. Floch, M. E. Tobar, *et al.*, "Generation of 103.75 GHz CW source with frequency instability using cryogenic sapphire oscillators," *IEEE Microwave Wireless Compon. Lett.* **22**, 85–87 (2012).
- S. B. Waltman, L. W. Hollberg, A. K. McIntosh, *et al.*, "Demonstration of a phase-lockable microwave to submillimeter wave sweeper," *Proc. SPIE* **2842**, 55–58 (1996).
- S. Fukushima, C. Silva, Y. Muramoto, *et al.*, "Optoelectronic millimeter-wave synthesis using an optical frequency comb generator, optically injection locked lasers, and a unitraveling-carrier photodiode," *J. Lightwave Technol.* **21**, 3043–3051 (2003).
- H.-J. Song, N. Shimizu, T. Furuta, *et al.*, "Broadband-frequency-tunable sub-terahertz wave generation using an optical comb, AWGs, optical switches, and a uni-traveling carrier photodiode for spectroscopic applications," *J. Lightwave Technol.* **26**, 2521–2530 (2008).
- T. Nagatsuma, H. Ito, and T. Ishibashi, "High-power rf photodiodes and their applications," *Laser Photonics Rev.* **3**, 123–137 (2009).
- A. Rolland, G. Ducournau, G. Danion, *et al.*, "Narrow linewidth tunable terahertz radiation by photomixing without servo-locking," *IEEE Trans. Terahertz Sci. Technol.* **4**, 260–266 (2014).
- T. M. Fortier, A. Rolland, F. Quinlan, *et al.*, "Optically referenced broadband electronic synthesizer with 15 digits of resolution," *Laser Photonics Rev.* **10**, 780–790 (2016).
- T. Tetsumoto, T. Nagatsuma, M. E. Fermann, *et al.*, "Optically referenced 300 GHz millimetre-wave oscillator," *Nat. Photonics* **15**, 516–522 (2021).
- E. A. Kittlaus, D. Elyahu, S. Ganji, *et al.*, "A low-noise photonic heterodyne synthesizer and its application to millimeter-wave radar," *Nat. Commun.* **12**, 4397 (2021).
- B. M. Heffernan, J. Greenberg, T. Hori, *et al.*, "Brillouin laser-driven terahertz oscillator up to 3 THz with femtosecond-level timing jitter," *arXiv* (2023).
- W. Jin, Q.-F. Yang, L. Chang, *et al.*, "Hertz-linewidth semiconductor lasers using cmos-ready ultra-high-Q microresonators," *Nat. Photonics* **15**, 346–353 (2021).
- C. Xiang, W. Jin, O. Terra, *et al.*, "3d integration enables ultralow-noise isolator-free lasers in silicon photonics," *Nature* **620**, 78–85 (2023).
- B. Li, W. Jin, L. Wu, *et al.*, "Reaching fiber-laser coherence in integrated photonics," *Opt. Lett.* **46**, 5201–5204 (2021).
- H. Cheng, N. Jin, Z. Dai, *et al.*, "A novel approach to interface high-Q Fabry-Pérot resonators with photonic circuits," *APL Photonics* **8**, 116105 (2023).
- Y. Liu, D. Lee, T. Nakamura, *et al.*, "Low-noise microwave generation with an air-gap optical reference cavity," *APL Photonics* **9**, 010806 (2024).
- I. Kudelin, W. Groman, Q.-X. Ji, *et al.*, "Photonic chip-based low-noise microwave oscillator," *Nature* **627**, 534–539 (2024).
- S. Sun, B. Wang, K. Liu, *et al.*, "Integrated optical frequency division for microwave and mmWave generation," *Nature* **627**, 540–545 (2024).
- J. Guo, C. A. McLemore, C. Xiang, *et al.*, "Chip-based laser with 1-hertz integrated linewidth," *Sci. Adv.* **8**, eabp9006 (2022).
- R. W. P. Drever, J. L. Hall, F. V. Kowalski, *et al.*, "Laser phase and frequency stabilization using an optical resonator," *Appl. Phys. B* **31**, 97–105 (1983).
- K. Numata, A. Kemery, and J. Camp, "Thermal-noise limit in the frequency stabilization of lasers with rigid cavities," *Phys. Rev. Lett.* **93**, 250602 (2004).
- M. L. Kelleher, C. A. McLemore, D. Lee, *et al.*, "Compact, portable, thermal-noise-limited optical cavity with low acceleration sensitivity," *Opt. Express* **31**, 11954–11965 (2023).
- A. Hati, C. W. Nelson, and D. A. Howe, "Pm noise measurement at w-band," *IEEE Trans. Ultrason. Ferroelectr. Freq. Control* **61**, 1961–1966 (2014).
- F. Bondu and O. Debieu, "Accurate measurement method of Fabry-Perot cavity parameters via optical transfer function," *Appl. Opt.* **46**, 2611–2614 (2007).
- S. Sun, M. W. Harrington, F. Tabatabaei, *et al.*, "Kerr optical frequency division with integrated photonics for stable microwave and mmwave generation," *arXiv* (2023).
- M. Endo and T. R. Schibli, "Residual phase noise suppression for Pound-Drever-Hall cavity stabilization with an electro-optic modulator," *OSA Contin.* **1**, 116 (2018).
- N. Jin, C. A. McLemore, D. Mason, *et al.*, "Micro-fabricated mirrors with finesse exceeding one million," *Optica* **9**, 965–970 (2022).
- J. Zang, X. Xie, Q. Yu, *et al.*, "Reduction of amplitude-to-phase conversion in charge-compensated modified unitraveling carrier photodiodes," *J. Lightwave Technol.* **36**, 5218–5223 (2018).